Optical scattering and backscattering by organic and inorganic particulates in U.S. coastal waters

William A. Snyder,[1,*] Robert A. Arnone,[2] Curtiss O. Davis,[3] Wesley Goode,[2] Richard W. Gould,[2] Sherwin Ladner,[2] Gia Lamela,[1] William J. Rhea,[1] Robert Stavn,[4] Michael Sydor,[5] and Allen Weidemann[2]

[1]Code 7230, U.S. Naval Research Laboratory, 4555 Overlook Avenue, S.W., Washington, D.C. 20375-5320, USA
[2]Code 7330, U.S. Naval Research Laboratory, Stennis Space Center, Mississippi 39529, USA
[3]College of Oceanic and Atmospheric Sciences, Oregon State University, 104 COAS Administration Building, Corvallis, Oregon 97331-5503, USA
[4]Department of Biology, University of North Carolina at Greensboro, 312 Eberhart Building, Greensboro, North Carolina 27402-6170, USA
[5]Department of Physics, University of Minnesota Duluth, 1023 University Drive, Duluth, Minnesota 55812-3009, USA
*Corresponding author: William.Snyder@nrl.navy.mil

Received 27 July 2007; revised 19 November 2007; accepted 21 November 2007; posted 27 November 2007 (Doc. ID 85804); published 5 February 2008

We present the results of a study of optical scattering and backscattering of particulates for three coastal sites that represent a wide range of optical properties that are found in U.S. near-shore waters. The 6000 scattering and backscattering spectra collected for this study can be well approximated by a power-law function of wavelength. The power-law exponent for particulate scattering changes dramatically from site to site (and within each site) compared with particulate backscattering where all the spectra, except possibly the very clearest waters, cluster around a single wavelength power-law exponent of -0.94. The particulate backscattering-to-scattering ratio (the backscattering ratio) displays a wide range in wavelength dependence. This result is not consistent with scattering models that describe the bulk composition of water as a uniform mix of homogeneous spherical particles with a Junge-like power-law distribution over all particle sizes. Simultaneous particulate organic matter (POM) and particulate inorganic matter (PIM) measurements are available for some of our optical measurements, and site-averaged POM and PIM mass-specific cross sections for scattering and backscattering can be derived. Cross sections for organic and inorganic material differ at each site, and the relative contribution of organic and inorganic material to scattering and backscattering depends differently at each site on the relative amount of material that is present.

OCIS codes: 010.1350, 010.4450, 010.4458.

1. Introduction

The inherent optical absorption, scattering, and backscattering properties of a water body define the way light propagates through the medium, and this information can be used to infer water properties from the remote sensing reflectance (R_{rs}) optical signal seen with remote sensing systems [1–5]. Because the scattering and absorption properties of phytoplankton, colored dissolved organic matter (CDOM), organic detritus, and mineral particles can have different wavelength dependencies [6–9], the wavelength dependence of R_{rs} provides clues to the nature and amount of these materials [3,10–14]. Uncoupling the R_{rs} signature requires knowledge of the absorption, scattering, and backscattering properties of the in-water material.

Current understanding of the absorption and scattering properties of water is based on measurements taken with *in situ* filtered and unfiltered absorption and attenuation meters. With general recognition and understanding of proper calibration and processing procedures [15] it is now possible to accurately

0003-6935/08/050666-12$15.00/0

compare data collected by many groups at different locations around the globe. The development of commercial *in situ* sensors for determination of backscatter is much more recent. Consequently, closure between a variety of backscattering instruments has been achieved only recently [16]. Because maturation of these technologies is recent, spectral studies of backscatter within natural environments are still rare [17–19], and the spectral properties of particulate scattering have been addressed mainly in an average, statistical sense [20–22].

We present a study of the particulate scattering and backscattering spectral properties of three U.S. coastal sites. The questions we address are (1) how does spectral scattering vary for different coastal waters (that is, what are the general spectral characteristics of the particulate scattering and backscattering signal), (2) can the particulate scattering, backscattering, and backscattering-to-scattering ratio (the backscattering ratio) be related to the amount of organic and inorganic material in the water, and (3) what does this tell us about the nature of the particulate scattering and backscattering signals and the relationship between the two?

2. Methods

Data were collected in three optically distinct regions: off the coast of New Jersey from 21 July through 2 August 2001, in the Northern Gulf of Mexico (in and around Mobile Bay, Alabama) from 19 to 25 May 2002, and in Monterey Bay, California, from 13 to 23 April 2003. Optical conditions at these sites range from relatively clear (Monterey Bay) to very turbid (Northern Gulf of Mexico). These three areas have a different mix of components that control the optical signature, providing an excellent data set for studying the scattering and backscattering properties for a broad range of coastal conditions.

The Long-Term Ecosystem Observatory at a 15 m depth (LEO-15) study area [23] off the coast of New Jersey is characterized by periods of upwelling and downwelling events that cause complex physical and biological changes throughout the offshore area and within the water column. Apart from a couple of measurements made within the Great Bay estuary, most of our measurements occurred 2–15 km offshore during separate downwelling events [24]. The optical properties at this site are controlled by phytoplankton, CDOM, and organic and inorganic particulate material resuspended from the bottom.

The 2002 Northern Gulf of Mexico study site in and around Mobile Bay is characterized by a shallow and extended shelf in which waters are usually high in suspended sediments. Two research vessels were deployed in this area. One ship, the R/V Ocean Color, sampled the waters bounded by Mobile Bay proper to the east and Horne Island to the west between the coast and the barrier islands located ~18 km offshore. A larger vessel, the R/V Pelican, sampled the deeper Gulf of Mexico waters ~10–20 km outside the barrier islands. Optical properties at this site are controlled mainly by inorganic particles from resuspended bottom material and a strong influence from CDOM and less so from phytoplankton.

The third study site was in Monterey Bay located on the west coast of the United States. The waters in the area are usually relatively clear with little suspended sediments. Monterey Bay is strongly influenced by coastal upwelling and downwelling events. Midway through our experiment there was a change in wind direction on 17 April. Normally this indicates a shift from downwelling to upwelling conditions, but during our study period we did not detect any significant differences in either the optical or physical properties of the water inside the Bay. Optical properties at Monterey are typically controlled by phytoplankton with only minor influences from CDOM and inorganic particles.

A. Optical Measurements

The majority of our measurements were made with an optical profiling package [25] with water bottles to collect simultaneous water samples at some depths. This package contains a pair of WET Labs (Western Environmental Technology Laboratory, Philomath, Oregon) ac-9 meters, one unfiltered and one pumping water through a 0.2 μm Gelman filter, for simultaneous absorption and attenuation measurements of dissolved and particulate matter, a HOBI Labs (Hydro-Optics, Biology, and Instrumentation Laboratories, Redmond, Washington) Hydroscat-6 (HS-6) for total backscattering measurements, a Sea-Bird Sealogger (Sea-Bird Electronics, Bellevue, Washington) conductivity-temperature-depth (CTD) profiler for salinity, depth, and temperature measurements and a WET Labs WETStar chlorophyll fluorometer for chlorophyll fluorescence. These instruments are configured on a Seabird rosette that carries up to eight water bottles that were used to collect water samples at specific depths for further analysis. Data are collected and recorded with a WET Labs Super Modular Ocean Data and Power System as a function of time for each of the instruments. Vendor-provided software is then used at a later date to reference the measurements to a common depth scale. As part of our standard processing, the data are smoothed with a median filter to a common set of 0.5 m independent depth intervals.

The filtered ac-9 is used to obtain absorption measurements of the CDOM (or gelbstoff a_g) at wavelengths of 412, 440, 488, 510, 532, 555, 650, 676, and 715 nm. This is then subtracted from the unfiltered ac-9 absorption data (identical wavelengths) to obtain measurements of particulate absorption, a_p ($= a - a_g$), and particulate scattering, b_p ($= c - c_g - a_p$, where c is the attenuation). A wavelength proportional scattering correction [26] is applied to the unfiltered ac-9 absorption measurement after first subtracting the gelbstoff absorption. This correction assumes that particulate absorption at 715 nm is zero and that the scattering phase function is the same at all wavelengths. We will show later that this assumption of a wavelength-independent phase function is not correct and conse-

quently the scattering amount at blue wavelengths is on average undercorrected. Since we do not have a detailed measurement of the scattering phase function it is impossible to apply an exact correction. We have, however, developed a procedure to estimate this effect by using the scattering light correction [Eq. (3)] of McKee *et al.* [27] and picking an appropriate Fournier–Forand phase function based on the experimentally derived backscattering ratio [28]. This process can be iterated until convergence is achieved, and, while it changes the best-fit results for some particulate scattering spectra, it does not change the information content of the figures nor the primary results and conclusions of this paper. Until the community reviews this procedure, we have elected to present results based on the community accepted standard ac-9 light scattering correction. The ac-9s were cleaned daily and calibrated several times per week by passing optically clean water (four-cartridge NANOpure system, Barnstead, Van Nuys, California) through the flow cells.

A Hydroscat-6 (HS-6) provides backscattering measurements at wavelengths of 442, 488, 532, 589, 620, and 671 nm. All Hydroscat-6 data have been sigma corrected (corrected for attenuation) by use of the ac-9 measurements and then a particulate backscattering (b_{bp}) spectrum is derived as described by Boss *et al.* [16].

These instruments were used to make all the in-water optical observations at LEO-15 in 2001 and Monterey Bay in 2003. They were also used onboard the R/V Pelican to take measurements in the Gulf of Mexico in 2002. During that time period, another vessel, the R/V Ocean Color, was also used to obtain an independent set of ac-9 and HS-6 optical profile measurements closer to shore. For these measurements, filtered (gelbstoff a_g) measurements were made only at the surface by placing the 0.2 μm filtered ac-9 instrument into the water to a depth of approximately 2–3 m and then taking the measurement. The unfiltered depth-profile data were then taken by removing the ac-9 from the water, removing the filter, and then lowering the ac-9 back into the water to obtain the depth profile. This measurement was then followed with the HS-6 optical profile measurements. The unfiltered depth profile data have been processed in a manner identical to that described above to obtain absorption, attenuation, and backscattering spectra at common 0.5 m depth intervals. Particulate a_p and b_p are estimated by assuming constant gelbstoff absorption with depth and subtracting the surface measured a_g value. Because of this assumption, all R/V Ocean Color particulate scattering and, to a much lesser degree backscattering, spectra, except for the surface measurements, must be treated with some caution. However, these waters are relatively shallow and well mixed and in general we believe these errors to be small. At no point is the scattering and backscattering spectral behavior of the R/V Ocean Color data taken at depths appreciably different from that seen at the surface. Comparisons with *in situ* water bottle surface measurements presented later use only the corresponding surface measured a, a_g, and c spectra. The total optical data set for all sites and instruments is greater than 6000 sets of gelbstoff and particulate absorption, and particulate attenuation, scattering, and backscattering spectra.

B. Water Samples

Water bottle samples were collected at some stations at each of the sites. This includes 21 samples for the LEO-15, 62 for the Northern Gulf of Mexico, and 71 for Monterey Bay, for a total of 154 water samples. When searching for relationships between optical and physical properties, we used the optical data taken at the same depth and time of the water sample measurements.

A suspended sediment analysis was performed for each water sample. Total suspended sediment (TSS) was obtained by measuring the difference in weight of pre-ashed, dried Whatman GF/F glass fiber filters with 0.7 μm nominal pore sizes before and after filtration of whole-water field samples. Samples were rinsed with 300 ml of de-ionized water following filtration and a salt correction [29] applied. The samples were then dried at 103 °C prior to weighing. To remove organic matter, the filter was then combusted at 550 °C. The amount of particulate inorganic matter (PIM) is the weight after combustion minus the ashed filter weight. Particulate organic matter (POM) is calculated as POM = TSS − PIM. The drying process essentially removes all the water from the sample, both external and internal to the cell. Thus our POM measurements represent only the nonhydrated (dry) mass of organic material present in the sample. As marine organisms are 80–95% water, the mass of the living organisms that make up this material will be much greater. POM, PIM, and TSS quantities are each converted to concentration (in units of grams per cubic meter) by dividing the particulate mass by the volume of water that was filtered.

For LEO-15, our estimate of the weight of the ashed filters could be systematically underestimated, and consequently our values for POM (PIM) systematically overestimated (underestimated) by as much as 0.5 g/m^3. Because of this, estimates for the POM to PIM ratio presented later could be uncertain for LEO-15 if POM or PIM values are small.

Water samples were also taken for measurement of chlorophyll a [Chl a] and other pigments by use of high-performance liquid chromatography (HPLC) analysis, which was done postdeployment. Water samples were filtered through 0.7 μm GF/F 25 mm glass fiber filters that were stored in liquid nitrogen and shipped to the Center for Hydro-Optics and Remote Sensing (CHORS), San Diego State University, for processing. In each case the samples were processed using the method of Wright *et al.* [30], following the NASA protocol for HPLC analysis [31]. This resulted in a uniformly processed set of chlorophyll a plus 22 other phytoplankton pigment concentration

measurements for each of our samples at the various sites.

3. Results

A. Site-Averaged Properties

The site-averaged optical and physical properties for the subset of data with simultaneous optical and physical measurements are listed in Table 1. The LEO-15 data have been separated into measurements made within the Great Bay estuary and those made offshore into time periods corresponding to different downwelling events. We will show later that the scattering optical properties differ for these time periods.

Scrutiny of Table 1 indicates that both optical and particulate values tend to be smallest for Monterey Bay and largest for the R/V Ocean Color measurements. The organic fraction (POM/TSS) of material in the water is smallest for Great Bay (7–10%), followed by the Northern Gulf of Mexico (27%) and the LEO-15 measurements of 1–2 August (34%) where inorganic material dominates, and is largest for the LEO-15 measurements taken 23 July (70%). The Monterey Bay organic and inorganic amounts are comparable, with the organic fraction averaging around 50%.

The particulate chlorophyll mass-specific absorption cross section $\{a_p(440)/[\text{Chl } a]\}$ is comparable at all sites, ranging on average from 0.06 to 0.15 m^2/mg. However, the amount of organic material per unit of chlorophyll, POM/[Chl a], varies greatly between the sites and is very large for the Northern Gulf of Mexico area. This suggests that the Northern Gulf of Mexico area has a larger proportion of organic detrital material in the water compared with the other sites.

Apart from its low salinity and overall larger physical and optical property values, there is no fundamental difference in the R/V Ocean Color (inshore of Horne Island) and R/V Pelican (offshore of Horne Island and in the Gulf of Mexico) particulate properties, at least during the time of our measurements. Organic fractions, POM/[Chl a] and a_p/[Chl a] are all similar. The intrusion of fresh water from the coast appears to have a negligible effect on the optical and physical properties over much of the area around the barrier islands. Resuspended bottom detrital and mineral materials dominate the optical and physical properties.

The Great Bay estuary and the offshore LEO-15 water properties are also similar to each other, apart from their organic fractions. Temperature and salinity values are particularly comparable, which indicates that the station at which the Great Bay measurements were taken (the narrow channel between Seven Islands to the West and the marsh lands to the East) is dominated by tidal coastal water and resuspended mineral particles.

B. Particulate Scattering Spectra

To provide a measure of the general wavelength dependence, we fit each particulate scattering spectrum to a power-law function of wavelength:

$$f(\lambda) = f_{550}(\lambda/550)^{\gamma}. \quad (1)$$

This fit provides the amplitude at 550 nm (f_{550}, in reciprocal meters) and a power-law exponent (γ, dimensionless units). A reference wavelength at 550 nm was chosen to compare our results more readily with those reported elsewhere [20–22]. Best-fit parameters and standard errors were derived by use of a linear regression analysis by taking the logarithm of Eq. (1). Although a wavelength-dependent structure can be exhibited in the individual spectra (see discussion later in this section), this structure, while statistically significant, is typically not large, and a power-law fit provides a good concise representation of the general spectral shape as a function of wavelength.

Table 1. Site-Averaged Simultaneous Optical and Physical Properties[a]

		Data Set						
Parameter	Units	LEO-15 23 July 2001	LEO-15 1–2 Aug 2001	Great Bay 27 July 2001	Great Bay 31 July 2001	R/V Pellcan 19–25 May 2002	R/V Ocolor 20–24 May 2002	Monterey Bay 13–23 July 2003
Salinity	PSU	30.8 (0.1)	31.1 (0.0)	31.1	30.9	31.7 (1.9)	19.9 (7.9)	33.3 (0.3)
Temperature	°C	23.1 (0.9)	21.6 (0.6)	20.6	21.0	23.0 (0.6)	21.6 (1.0)	11.8 (0.8)
$a_g(412)$	m^{-1}	0.46 (0.07)	0.34 (0.05)	0.29	0.80	0.48 (0.22)	0.96 (0.53)	0.11 (0.02)
$a_p(440)$	m^{-1}	0.29 (0.04)	0.21 (0.04)	0.50	0.34	0.26 (0.19)	0.56 (0.38)	0.15 (0.09)
$b_p(532)$	m^{-1}	2.95 (0.80)	3.87 (1.39)	3.60	3.02	2.02 (1.55)	5.08 (2.69)	0.52 (0.31)
$b_{bp}(532)$	m^{-1}	0.026 (0.011)	0.034 (0.020)	0.041	0.073	0.049 (0.050)	0.114 (0.078)	0.008 (0.008)
b_{bp}/b_p	—	0.009 (0.002)	0.008 (0.002)	0.011	0.023	0.020 (0.008)	0.021 (0.006)	0.011 (0.004)
PIM	g/m^3	0.12	1.25 (0.62)	1.90	4.62	2.7 (1.4)	4.8 (2.2)	0.5 (0.8)
POM	g/m^3	0.32	0.62 (0.33)	0.13	0.51	0.9 (0.3)	1.8 (0.8)	0.3 (0.2)
POM/TSS	—	0.70	0.34 (0.18)	0.07	0.10	0.26 (0.07)	0.28 (0.10)	0.52 (0.22)
[Chl a]	mg/m^3		8.7 (2.8)	7.9	3.2	2.1 (1.3)	5.6 (5.1)	2.7 (1.8)
POM/[Chl a]	—		69.7 (28.9)	16.8	159.0	523.3 (281.2)	446.2 (196.5)	141.5 (108.2)
a_p/[Chl a]	m^2/mg		0.06 (0.01)	0.06	0.11	0.15 (0.14)	0.12 (0.04)	0.06 (0.03)

[a]Sample deviations are listed in parenthesis. Values without sample deviations indicate a single measurement.

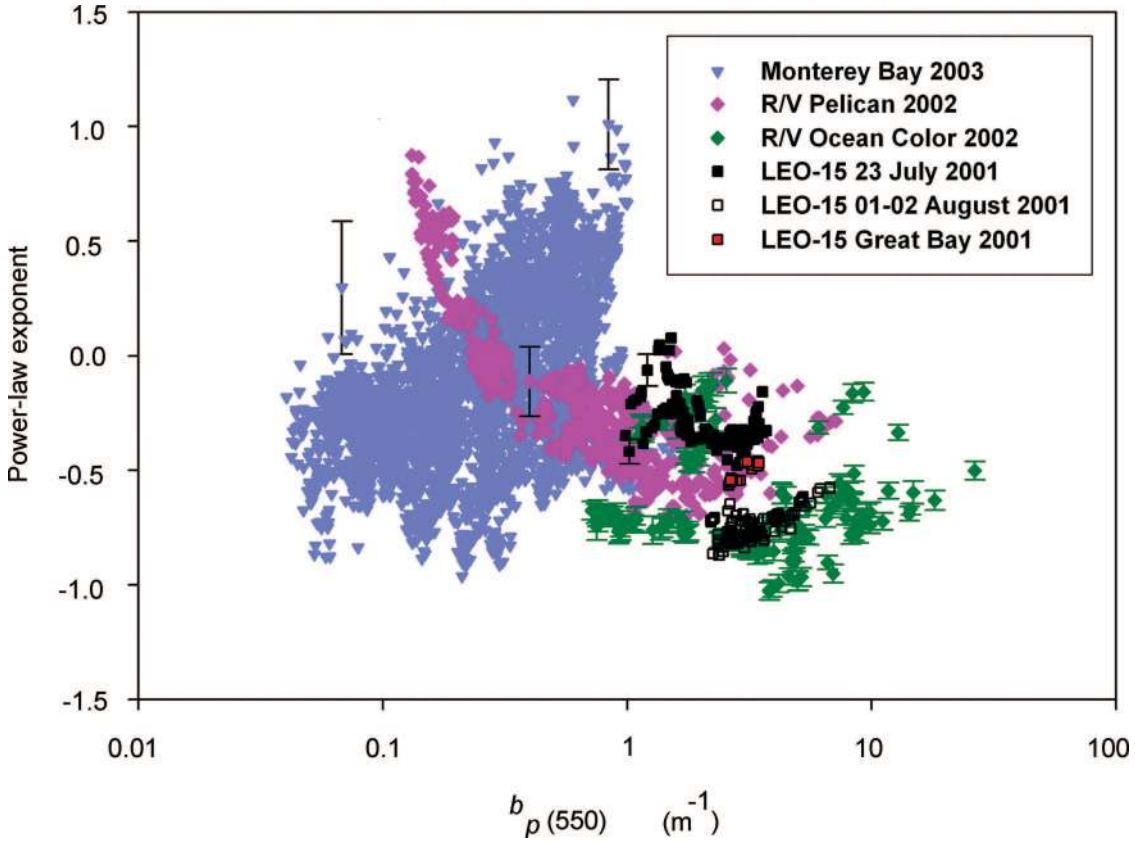

Fig. 1. Result of fitting all the ac-9 total particulate scattering (b_p) spectra to a power-law function of wavelength. Plotted is the best-fit amplitude at 550 nm and the power-law exponent for each fit. The x-axis values are plotted on a logarithmic scale. Because of the high density of points, uncertainties are shown only for the R/V Ocean Color measurements and other representative data points.

The results of using Eq. (1) to fit all the ac-9 particulate scattering (b_p) data for LEO-15 2001, Northern Gulf of Mexico (R/V Pelican and R/V Ocean Color) 2002, and Monterey Bay 2003 to a power-law function of wavelength are shown in Fig. 1, where the power-law spectral exponent (γ) is plotted as a function of the best-fit amplitude at 550 nm for each spectral fit. There is considerable variation in the spectral exponent with values ranging from approximately $+1.0$ to -1.0. Positive spectral exponents are observed only for $b_p(550) < 1\ \mathrm{m}^{-1}$, and even then approximately two thirds of the total number of spectra below this limit exhibit a negative spectral exponent that can be as steep as -1. At greater particulate scattering amounts, γ is typically negative and can range between 0 and -1.

How well does a power-law function describe the shape of the particulate scattering spectrum? While it is beyond the scope of this research to undertake a detailed study of the shape of each spectrum, it is possible to obtain at each wavelength a measure of the average degree of deviation from a simple power-law form and to quantify the degree of variation between individual spectra. This is accomplished by measuring at each wavelength the fractional difference of the observed signal from that expected using the best-fit power-law functional form, that is,

$$\text{fractional difference}(\lambda) = \frac{f_{\text{obs}}(\lambda) - f_{\text{pred}}(\lambda)}{f_{\text{pred}}(\lambda)}, \quad (2)$$

where f_{obs} is the measured value at each wavelength and f_{pred} is the predicted value obtained with best-fit parameters.

The average fractional difference and standard deviation at each wavelength are plotted in Fig. 2 for each site. For the most part, the average fractional difference is less than 0.05 (5%) at each wavelength although the standard deviations range from $\sim$0.01 to $\sim$0.10. A fractional change of 0.010, 0.027, 0.007, and 0.095 is on average statistically significant at the 90% confidence level for individual LEO-15 2001, R/V Pelican (Northern Gulf of Mexico) 2002, R/V Ocean Color (Northern Gulf of Mexico) 2002, and Monterey Bay 2003 spectra, respectively. This estimate is based on our using a value of 0.03 m^{-1} for the 90% uncertainty in each of our individual ac-9 particulate scattering values and dividing this number by the site-averaged particulate scattering value at each wavelength. This uncertainty estimate is based on a statistical analysis of the distribution of individual ac-9 points about the 0.5 m binned data used in our sample. Thus, a statistically significant structure is likely in many of the individual particulate scat-

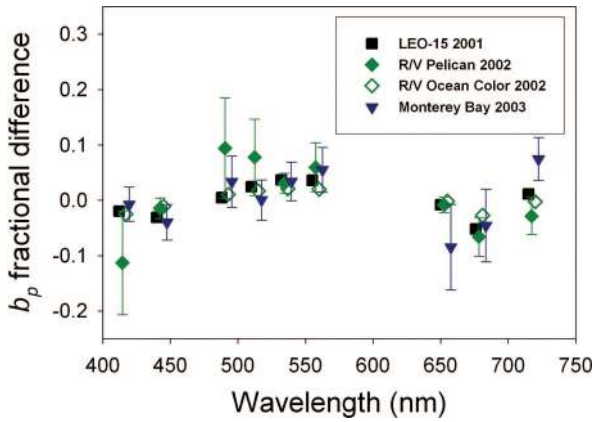

Fig. 2. (Color online) Average fractional difference and standard deviation of individual particulate scattering spectra from a power-law function of wavelength for each major data group. For some data points the standard deviation is of the order of the size of the data symbol or smaller. Fractional differences are typically less than 10% at each ac-9 wavelength. A small wavelength shift has been applied to the data to avoid overlap.

tering spectra, but deviations from a power law are typically less than 10% of the fitted value. The negative fractional differences at 412, 440, and 676 nm correspond to peaks in the organic particulate absorption spectra (see Fig. 9), and the structure seen here probably results from the absorption of light by pigmented organic particles.

C. Particulate Backscattering Spectra

The result of fitting the particulate backscattering spectral data to a power-law function of wavelength is shown in Fig. 3. Here, the power-law exponent (γ) is plotted as a function of the best-fit amplitude [$b_{bp}(550)$] at 550 nm. The 488 and 532 nm Hydroscat-6 channels were obviously bad for the LEO-15 2001 data, and these two wavelengths have not been included in any of the backscattering spectral fits for any of the data presented here. [If we were to include these two wavelengths where we have good data for the Northern Gulf of Mexico, this would have a small effect on the best-fit power-law exponent, steepening it on average by 0.09 and 0.03 for the R/V Pelican and R/V Ocean Color data, respectively. The change in exponent for Monterey Bay data is more pronounced, steepening it by ~0.5.]

Unlike the particulate scattering data that display a wide range in spectral exponent for a particular scattering amount, the individual particulate backscattering measurements are statistically consistent [the chi-square per degree of freedom (χ_v^2) = 1.00] with a single value of γ for $0.005\ \mathrm{m}^{-1} < b_{bp}(550) < 0.015\ \mathrm{m}^{-1}$. For these data the mean power-law exponent and standard deviation of the data are -0.942 ± 0.210. However, scrutiny of individual depth profiles indicates that the spread in this value is not random and represents small, but real, spectral changes in the backscattering spectral properties of the water.

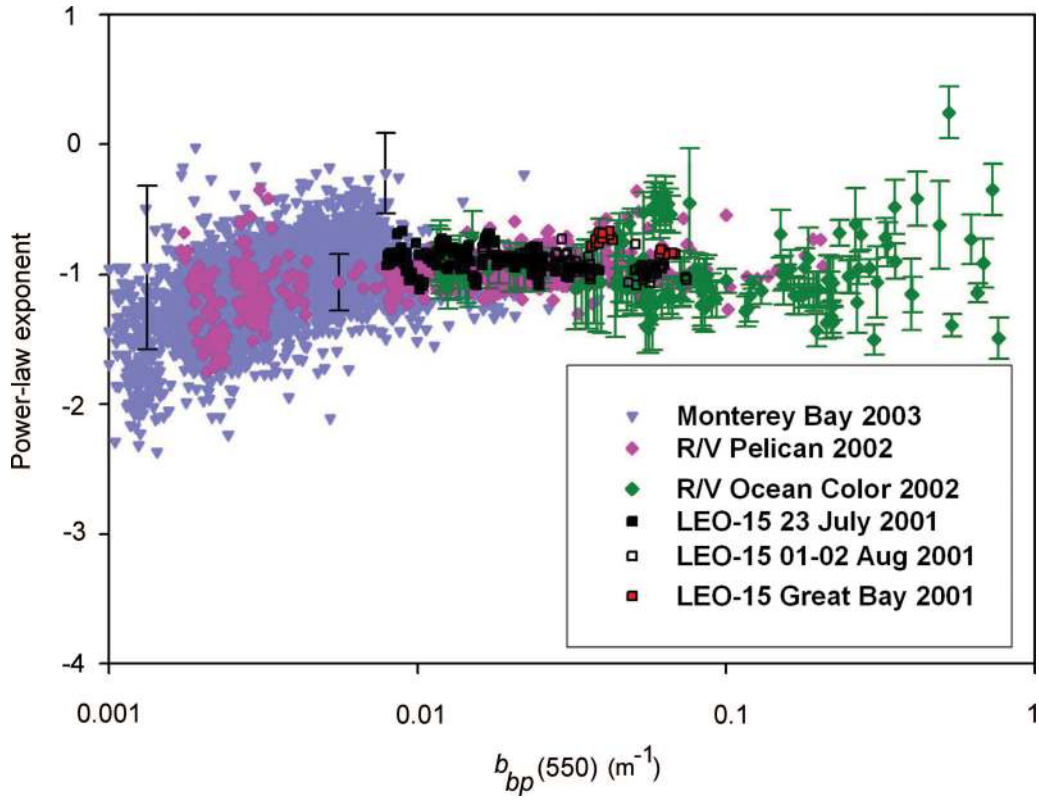

Fig. 3. Result of fitting all the HS-6 particulate backscattering (b_{bp}) spectra to a power-law function of wavelength. Plotted is the best-fit amplitude at 550 nm and the power-law exponent for each fit. The x-axis values are plotted on a logarithmic scale. Because of the high density of points, uncertainties are shown only for the R/V Ocean Color measurements and other representative data points.

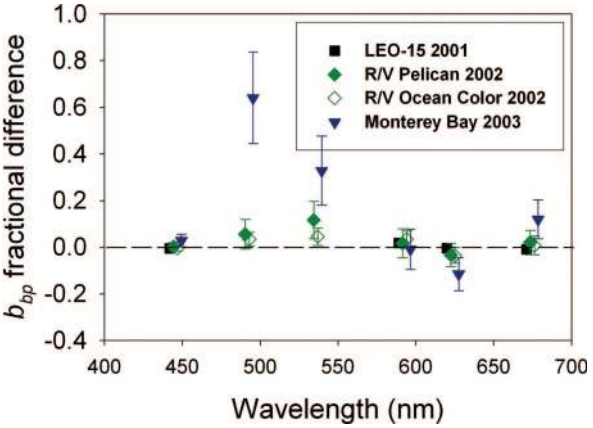

Fig. 4. (Color online) Average fractional difference and standard deviation of individual particulate backscattering spectra from a power-law function of wavelength for each major data group. Fractional differences are typically less than 10% at each HS-6 wavelength although much larger departures are evident for the Monterey Bay averages at some wavelengths. A small wavelength shift has been applied to the data to avoid overlap.

There does appear to be on average a steepening of the power-law exponent (γ becomes more negative) for $b_{bp}(550)$ less than $\sim 0.005\ m^{-1}$. However, for these points the particulate backscattering is comparable to that of pure water, and the pure water subtraction applied to the HS-6 data will have a noticeable effect on the resultant particulate backscattering spectral shape. At these low levels of particulate backscattering, the average power-law exponent could be consistent with the average value seen at higher backscattering levels if our pure water backscattering correction [32] is reduced by $\sim 15\%$. This reduction makes the pure water values consistent with those measured by others [33]. Thus it remains unresolved at this point if the downward trend in spectral exponent below $b_{bp}(550) \sim 0.005\ m^{-1}$ is real.

The average spectral fractional differences from a power-law function of wavelength at each site are plotted in Fig. 4. A fractional change of 0.080, 0.091, 0.014 and 0.631 is on average statistically significant for individual LEO-15 2001, R/V Pelican (Northern Gulf of Mexico) 2002, R/V Ocean Color (Northern Gulf of Mexico) 2002, and Monterey Bay 2003 spectra, respectively. In this case, an uncertainty of $0.006\ m^{-1}$ in the individual 0.5 m binned HS-6 backscattering values was used. The average fractional differences are typically smaller than this. Thus, a statistically significant structure is unlikely to be evident in most of the individual backscattering spectra. Figure 4 does suggest, however, that the average backscattering spectrum for Monterey Bay 2003 will depart significantly from a simple power-law functional form. Note that the LEO-15 and Northern Gulf of Mexico data, sites that are dominated more by detrital and/or inorganic particulates, do not show the strong spectral deviations as in Monterey Bay where biological particles dominate.

D. Particulate Backscattering Ratio

The backscattering ratio $\tilde{b}_{bp}$ ($= b_{bp}/b_p$) could in theory provide a measure of the degree of particulate organic and inorganic material present in the water [34]. The wavelength dependence of the backscattering ratio is of theoretical importance because standard models predict that the backscattering ratio will be independent of wavelength. On a practical note, determination of the backscattering ratio wavelength dependence is of importance because the standard light scattering correction of attenuation meter data assumes there is no spectral dependence. We have shown that the properties of both the particulate scattering and the backscattering spectra can be generally represented by simple power-law functions of wavelength. We can use this to quantify the spectral dependence of the backscattering ratio for these data. Then, the wavelength dependence of the backscattering ratio is given by

$$\tilde{b}_{bp}(\lambda) = \frac{b_{bp}(\lambda)}{b_p(\lambda)} = \tilde{b}_{bp}(550)(\lambda/550)^{\gamma}, \qquad (3)$$

where $\tilde{b}_{bp}(550) = b_{bp}(550)/b_p(550)$, and $\gamma = \gamma_{bbp} - \gamma_{bp}$ and $\gamma_{bbp}(\gamma_{bp})$ are the power-law exponents of the particulate backscattering (scattering) spectral fit. Standard propagation of error formulas are used to assign parameter uncertainties.

The backscattering ratio exponent γ is plotted as a function of the backscattering ratio at 550 nm for all our data in Fig. 5. Identical results are obtained if a power-law function is directly fit to the measured b_{bp}/b_p ratio data. The backscattering ratio at 550 nm varies from ~ 0.005 to 0.06. The wavelength dependence of this ratio varies from site to site and within each site.

Many of the Northern Gulf of Mexico 2002 R/V Ocean Color spectra are consistent with an exponent that varies within a narrow range about $\gamma \sim -0.3$ over the complete 0.01–0.06 $\tilde{b}_{bp}(550)$ range of that data. The spectral exponent for the 23 July and 1–2 August 2001 LEO-15 data bracket this value, although on 23 July (1–2 August) $\gamma = -0.62 \pm 0.13$ (-0.14 ± 0.14). For these days the spectral index averages to -0.38 ± 0.27, but $\chi_v^2 = 12.5$ is inconsistent with a constant value. The change in spectral index must reflect a change in the water properties. The organic fractions (POM/TSS) on these days are different (Table 1), if the single suspended sediment 23 July measurement is representative of the complete set of observations, and it may be that the steeper exponent on 23 July is due to a larger organic fraction.

The ranges in the spectral exponent for the R/V Pelican Northern Gulf of Mexico 2002 and Monterey Bay 2003 measurements are broadly similar to each other and cover a larger range than LEO-15 2001 and R/V Ocean Color 2002. The range in $\tilde{b}_{bp}(550)$ for these data sets is also similar. Below $\tilde{b}_{bp}(550) \sim 0.025$ the backscattering ratio spectral exponent

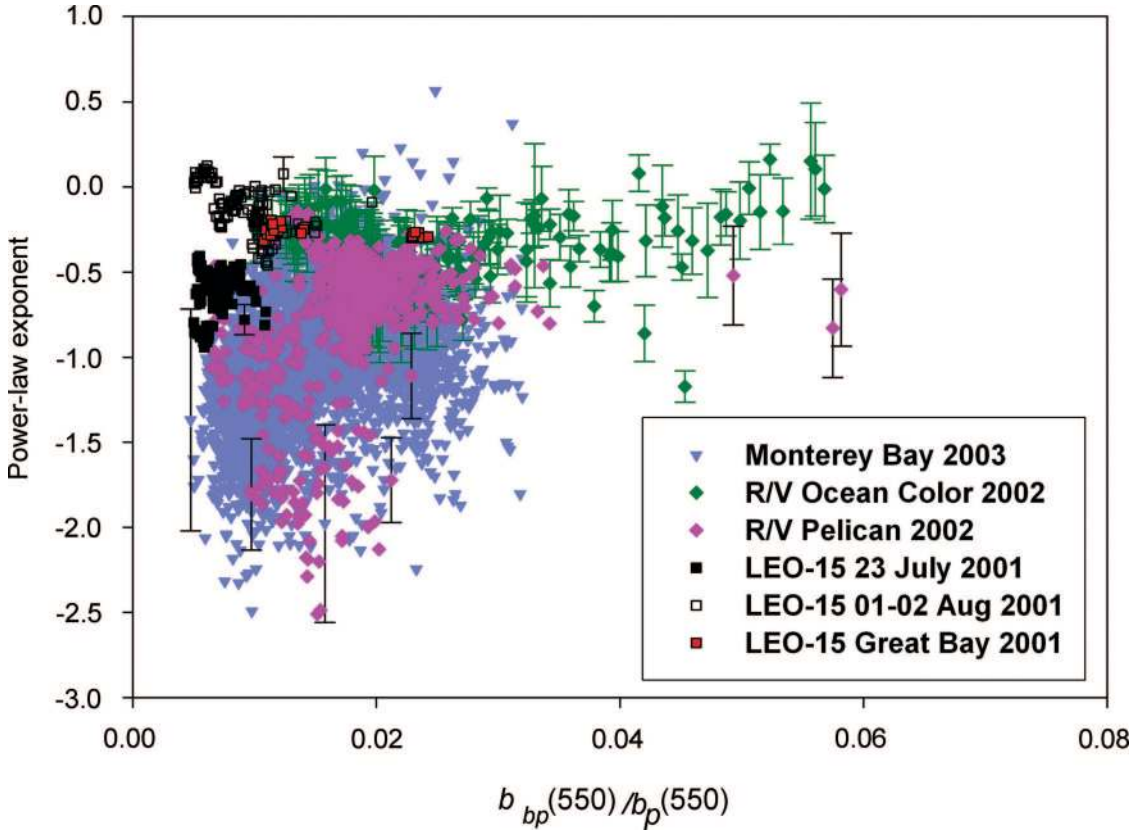

Fig. 5. Particulate backscattering ratio spectral exponent plotted as a function of backscattering ratio at 550 nm. Because of the high density of points, uncertainties are shown only for the R/V Ocean Color measurements and other representative data points.

becomes more negative as the backscattering ratio becomes smaller. An *F*-test analysis [35] indicates this downward trend is significant at the approximately 98% level in both data sets. Inspection of individual casts indicates that for Monterey Bay this represents a systematic downward trend for $\tilde{b}_{bp}(550) < 0.02$. The change is not as systematic for the R/V Pelican data where in some cases the spectral exponent becomes flatter (less negative) as $\tilde{b}_{bp}(550)$ decreases to very low values.

Just a few of our measurements exhibit a constant ($\gamma = 0$) or rising ($\gamma > 0$) backscattering ratio. For most of our spectra, a backscattering ratio that decreases to longer wavelengths is the norm. Wavelength-dependent backscattering ratios have been reported for data collected in the Irish and Celtic Seas [18] and the Black Sea [17,36]. A study [37] of Crater Lake, New York Bight, southern California/Mexico, and Gulf of California coastal sites, however, reports no statistical evidence for a wavelength-dependent backscattering ratio.

E. Relationship of $\tilde{b}_{bp}(550)$ to Bulk Water Composition

The backscattering ratio for light scattered from uniform spherical particles (Mie scattering) depends on the index of refraction of the material and is larger for high index of refraction mineral particles than for low index of refraction organic particles. If the net index of refraction (that is, bulk composition) of the water is the dominant factor governing the backscattering ratio, the backscattering ratio should be related to the organic and inorganic mix of the water.

To test this hypothesis, we plotted $\tilde{b}_{bp}(550)$ as a function of the organic fraction of the material in the water in Fig. 6. There is no statistically significant correlation when the data are considered either as a group or from individual sites. Negative results are also found for other permutations of

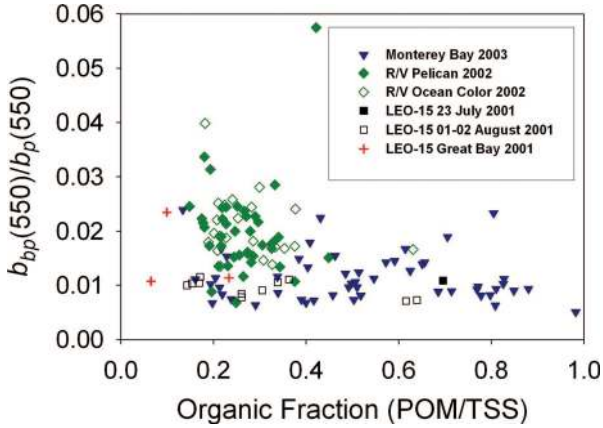

Fig. 6. (Color online) Particulate backscattering ratio at 550 nm plotted as a function of the organic fraction of material. There is no correlation in the data when treated either as a group or from individual sites.

POM, PIM, and TSS. This is similar to the result reported by Loisel *et al.* [38], who found no general correlation between the backscattering ratio at 650 nm and the particulate organic carbon (POC) to TSS ratio in English Channel and North Sea data, although they did find a correlation in a limited (an individual transect) data subset. They did report a weak correlation between the 650 nm backscattering ratio and the POC/[Chl a] ratio, something that is not statistically evident in our own $\tilde{b}_{bp}(550)$ versus POM/[Chl a] comparison (not shown).

Loisel *et al.* [38] noted that the presence of detrital particles appears to enhance the backscattering ratio and there are examples in our data set for which this appears to be the case. The 27 and 30 July 2001 measurements in Great Bay (Table 1) are a case in point, where organic fractions are similar (~0.1) but with the 30 July measurement having larger backscattering and POM/[Chl a] ratios. The Northern Gulf of Mexico data also have on average higher backscattering ratios and both higher mineral fractions and POM/[Chl a] ratios. Within a given data set, however, there is no discernible evidence that the largest backscattering ratios are on average associated with both higher mineral fractions and higher POM/[Chl a] ratios. This suggests that other factors (e.g., particle size and/or shape) must also influence the backscattering ratios observed in our data.

F. Mass-Specific Scattering, Backscattering, and Absorption Coefficients

Particulate scattering (b_p), backscattering (b_{bp}), and absorption (a_p) should be related to POM and PIM, and this can be used to derive the average mass-specific cross sections for particulate organic and inorganic material in each of these waters. The particulate scattering, for example, can be partitioned into an organic and inorganic contribution:

$$b_p = \mathrm{POM}\ \sigma_{bp,\mathrm{POM}} + \mathrm{PIM}\ \sigma_{bp,\mathrm{PIM}}, \tag{4}$$

where $\sigma_{bp,\mathrm{POM}}$ ($\sigma_{bp,\mathrm{PIM}}$) is the organic (inorganic) mass-specific particulate scattering cross section (in square meters per grams). Similar equations hold for particulate backscattering and absorption. The measured optical coefficients at each wavelength are then divided by the measured POM (or PIM) amounts and a linear correlation of b_p/POM (or b_p/PIM) with PIM/POM (or POM/PIM) for each data set is used to define the slope and intercept (that is, derive the mass-specific organic and inorganic cross sections) along with their standard uncertainties. The mass-specific cross sections derived with the PIM/POM and POM/PIM correlations are not identical but overlap within their uncertainties. In choosing a solution we present the linear regression result with the largest linear regression coefficient, that is, the smallest probability (P) of a false positive correlation, and the smallest overall uncertainty in the estimate of the organic and inorganic values. These cross sections provide the best overall match to the set of station measurements

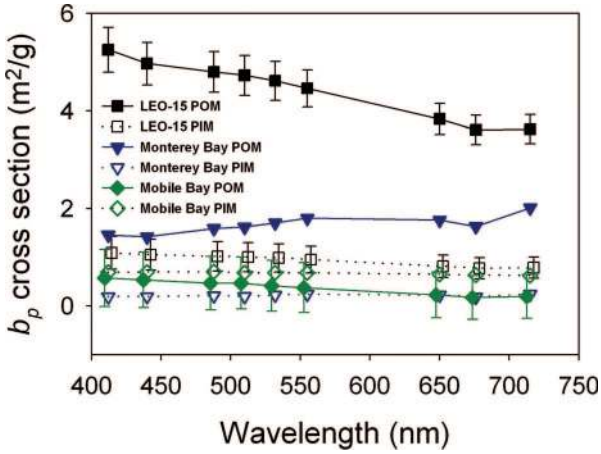

Fig. 7. (Color online) Site-averaged particulate scattering mass-specific cross sections for POM and PIM for each site. For some data points the uncertainty is of the order of the size of the data symbol or smaller. A small wavelength shift has been applied to the data to avoid overlap. The POM cross section at LEO-15 is high when compared with theoretical calculations and values reported in the literature. Given the uncertainty in filter pad correction for this site, the LEO-15 results should be treated with caution.

but may not necessarily provide a statistically good fit to measurements at any single station if the station particulate properties are not a good match with the data set average.

The organic and inorganic mass-specific cross sections for particulate scattering, backscattering, and absorption are presented in Figs. 7–9, respectively. All the correlations used to derive these results were significant; $P = 10^{-3}$ was the largest value. In some cases our best-fit estimates are slightly negative and/or parameter uncertainties overlap zero (0). In these cases the error bars show that the estimate is not statistically different from zero and place upper limits to these estimates. Our results are generally consistent with those measured by others [9,39–42]. The organic (inorganic) backscattering ratios at 550 nm of 0.006, 0.010, and <0.043 (0.016, 0.027, and

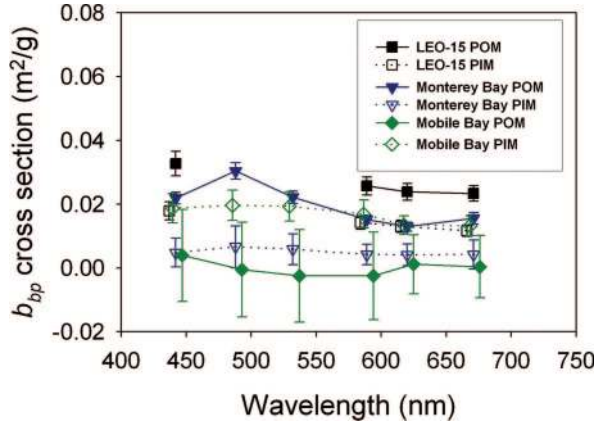

Fig. 8. (Color online) Site-averaged particulate backscattering mass-specific cross sections for POM and PIM for each site. A small wavelength shift has been applied to the data to avoid overlap. The LEO-15 results should be treated with caution.

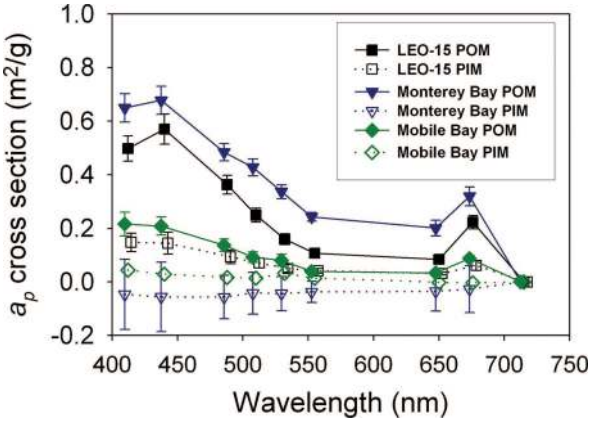

Fig. 9. (Color online) Site-averaged particulate absorption mass-specific cross sections for POM and PIM for each site. For some data points the uncertainty is of the order of the size of the data symbol or smaller. A small wavelength shift has been applied to the data to avoid overlap. The LEO-15 results should be treated with caution.

0.024) for LEO-15, Monterey Bay, and Northern Gulf of Mexico, respectively, are consistent with those expected for organic and mineral particles. The absorption of light by mineral particles (Fig. 9), although small, is not necessarily zero. There is a small 676 nm feature indicative of organic material in the inorganic absorption cross section for LEO-15 (Fig. 9), and it is possible that for this site there may not be a complete separation of components.

At 550 nm, the average mass-specific particulate scattering cross section for organic material at Monterey Bay is approximately a factor 10 larger than for inorganic material. For LEO-15 it is a factor of 5. The corresponding backscattering cross-sectional ratios are approximately 3 and 2, respectively. Thus for Monterey Bay, unless PIM greatly exceeds POM, the organic material in the water will dominate the particulate scattering, and particulate backscattering will more comparably reflect both the organic and the inorganic matter that is present. The situation for LEO-15 appears similar to Monterey Bay although more balanced. The mass-specific scattering cross section for POM at LEO-15 (Fig. 7) is high when compared with Mie theoretical calculations and values reported in the literature [22]. Given the uncertainty in the filter pad correction as described in Section 2, the LEO-15 result should be treated with caution.

For the Northern Gulf of Mexico the organic matter mass-specific cross sections for scattering and backscattering are at best comparable with or less than the inorganic cross sections. The mass-specific absorption cross section (Fig. 9) for organic material in the Northern Gulf of Mexico is approximately half of that for either LEO-15 or Monterey Bay and does not exhibit the turndown below 440 nm that is indicative of pigment absorption from living material. All our organic cross sections can have contributions from detrital as well as living material. The Northern Gulf of Mexico appears to have a larger detrital fraction than the other two sites, and its smaller organic cross sections for scattering, backscattering, and absorption probably reflect this larger detrital fraction.

4. Discussion

Three distinct coastal waters ranging from near oceanic (Monterey Bay) with modest but comparable amounts of organic and inorganic material, coastal margin (LEO-15) with more moderate and variable levels of material, to very turbid (Northern Gulf of Mexico) with large amounts of both suspended detrital and mineral particles were examined in this study.

We find a considerable degree of variation in the particulate scattering spectra. Not only are there differences between sites, but differences are readily apparent within a site. Our average particulate scattering power-law spectral exponent is -0.48, although variations from -1.0 to $+1.0$ are seen in our complete sample. However, all our particulate backscattering spectra, except possibly for the very clearest waters (Monterey Bay and offshore Gulf of Mexico), are more narrowly distributed about a power-law exponent of -0.94.

The differences in scattering and backscattering spectral behavior and the resulting wavelength dependence to the backscattering ratio are the most striking aspects of our spectral study. Models that describe the bulk composition of water as a uniform mix of homogeneous spherical particles with Junge-like power-law distributions over all particle sizes [34,43] do not predict this type of spectral behavior. In these models the backscattering ratio is always predicted to be independent of wavelength. Such models are not supported by our observations.

Particulate scattering at optical wavelengths responds predominantly to particles in the 1–10 μm range [44] and is sensitive to the internal constituency (that is, index of refraction) of those particles [34,44]. In the multiple component model of Stramski *et al.* [10] the particle size distribution is composed of a variety of phytoplankton components ranging in size from one to tens of micrometers, each with a differing wavelength-dependent scattering and backscattering cross section. The resultant particulate scattering spectral index then depends on the relative mix of the various components.

We observe a wide range of variation in the scattering power-law spectral exponent for any given particulate scattering magnitude. This suggests that the particulate scattering signature originates from a superposition of a set of spectrally different but optically comparable components whose makeup, shape, fractional abundance, and size may change from site to site, station to station, and/or over time.

Backscattering efficiency is inversely related to the size of the particle, and small detritus and/or mineral particles could dominate the backscattering signal in coastal waters [44]. In the Stamski *et al.* [10] model the detrital and mineral particle size distributions are the same and both exhibit a power-law backscat-

tering wavelength dependence with $\gamma = -0.91$. This value is almost identical to what we measure for $b_{bp}(550) > 0.005\ m^{-1}$. However, living organic particles can also contribute to the backscattering signal. In Monterey Bay, the spectral structure due to absorption by pigmented particles (Fig. 9) is reflected in the shape of the backscattering spectrum (Figs. 4 and 8). Contributions by living organic particles may also account for the small changes in the backscattering spectral exponent observed for $b_{bp}(550) > 0.01\ m^{-1}$ and for the larger spectral changes seen at smaller backscattering values.

Our results indicate that particulate scattering and backscattering in coastal environments are complex and appear dependent on the specific nature and relative composition of the particles that are present. The average mass-specific cross sections for organic and inorganic particles is different at each site and the relative contribution of organic and inorganic material to scattering and backscattering depends differently at each site on the relative amount of material that is present.

The average backscattering ratios for organic and inorganic material derived from the mass-specific cross sections are consistent with theoretical values. This suggests that at least on average the backscattering ratio should broadly reflect the relative composition of the water. Yet we failed to find such a relationship when we compared the measured backscattering ratio with the organic fraction of material as derived from PIM and POM. It may be that there are errors in at least some of our estimates or that our sample is too small to discern this relationship. Another possibility is that the filter pad measurements collect only those particles whose size is greater than $\sim 0.7\ \mu m$, and particles below this limit that contribute to the scattering and/or backscattering signal will not be measured. For a power-law size distribution of spherical particles whose number density varies as $R^{-3.5}$ (where R is the radius of the particle), the number of particles in the 0.1–0.7 μm range is more than 100 times greater than in the 0.7–10 μm range. The particle mass, however, is only approximately one-fourth. If scattering and backscattering respond differently to particles below 0.7 μm, filter pad mass measurements might not provide an appropriate measure of the relative contribution of organic and inorganic material to the backscattering ratio.

We thank Chuck Trees and the staff at CHORS for processing the HPLC data and David Dana for enumerable e-mails that involved Hydroscat-6 processing. We also thank the Office of Naval Research for supporting this research.

References

1. V. E. Brando and A. G. Dekker, "Satellite hyperspectral remote sensing for estimating estuarine and coastal water quality," IEEE Trans. Geosci. Remote Sens. **41,** 1378–1387 (2003).
2. H. M. Dierssen, R. C. Zimmerman, R. A. Leathers, T. V. Downes, and C. O. Davis, "Ocean color remote sensing of seagrass and bathymetry in the Bahamas Banks by high resolution airborne imagery," Limnol. Oceanogr. **48,** 444–455 (2003).
3. Z. P. Lee, K. L. Carder, S. K. Hawes, R. G. Steward, T. G. Peacock, and C. O. Davis, "Model for interpretation of hyperspectral remote-sensing reflectance," Appl. Opt. **33,** 5721–5732 (1994).
4. S. Maritorena, A. Morel, and B. Gentili, "Diffuse reflectance of oceanic shallow waters: influence of water depth and bottom albedo," Limnol. Oceanogr. **39,** 1689–1703 (1994).
5. C. D. Mobley, "Estimation of the remote-sensing reflectance from above-surface measurements," Appl. Opt. **38,** 7442–7455 (1999).
6. M. S. Twardowski, E. Boss, J. M. Sullivan, and P. L. Donaghay, "Modeling the spectral shape of absorption by chromophoric dissolved organic matter," Mar. Chem. **89,** 69–88 (2004).
7. A. Bricaud, H. Claustre, J. Ras, and K. Oubelkheir, "Natural variability of phytoplanktonic absorption in oceanic waters: influence of the size structure of algal populations," J. Geophys. Res. **109,** C11010, doi:10.1029/2004JC002419 (2004).
8. D. Stramski, E. Boss, D. Bogucki, and K. J. Voss, "The role of seawater constituents in light backscattering in the ocean," Prog. Oceanogr. **61,** 27–56 (2004).
9. E. A. Gallie and P. A. Murtha, "Specific absorption and backscattering spectra for suspended minerals and chlorophyll-a in Chilko Lake, British Columbia," Remote Sens. Environ. **39,** 103–118 (1992).
10. D. Stramski, A. Bricaud, and A. Morel, "Modeling the inherent optical properties of the ocean based on the detailed composition of the planktonic community," Appl. Opt. **40,** 2929–2945 (2001).
11. C. Dupouy, H. Loisel, J. Neveux, S. L. Brown, C. Moulin, J. Blanchot, A. Le Bouteiller, and M. R. Landry, "Microbial absorption and backscattering coefficients from in situ and POLDER satellite data during an El Niño–Southern Oscillation cold phase in the equatorial Pacific (180°)," J. Geophys. Res. **108**(C12), 8138, doi:10.1029/2001JC001298 (2003).
12. M. A. Moline, S. M. Blackwell, R. Chant, M. J. Oliver, T. Bergmann, S. Glenn, and O. M. E. Schofield, "Episodic physical forcing and the structure of phytoplankton communities in the coastal waters of New Jersey," J. Geophys. Res. **109,** C12S05, doi:10.1029/2003JC001985 (2004).
13. R. W. Gould, R. A. Arnone, and M. Sydor, "Absorption, scattering, and remote-sensing reflectance relationships in coastal waters: testing a new inversion algorithm," J. Coastal Res. **17,** 328–341 (2001).
14. M. Sydor, B. D. Wolz, and A. M. Thralow, "Spectral analysis of bulk reflectance from coastal waters: deconvolution of diffuse spectra due to scattering and absorption by coastal water," J. Coastal Res. **18,** 352–361 (2002).
15. M. S. Twardowski, J. M. Sullivan, P. L. Donaghay, and J. R. V. Zaneveld, "Microscale quantification of the absorption by dissolved and particulate material in coastal waters with an ac-9," J. Atmos. Ocean. Technol. **16,** 691–707 (1999).
16. E. Boss, W. S. Pegau, M. Lee, M. Twardowski, E. Shybanov, G. Korotaev, and F. Baratange, "Particulate backscattering ratio at LEO 15 and its use to study particle composition and distribution," J. Geophys. Res. **109,** C01014, doi: 10.1029/2002JC001514 (2004).
17. M. Chami, E. B. Shybanov, T. Y. Churilova, G. A. Khomenko, M. E.-G. Lee, O. V. Martynov, G. A. Berseneva, and G. K. Korotaev, "Optical properties of the particles in the Crimea coastal waters (Black Sea)," J. Geophys. Res. **110,** C11020, doi:10.1029/2005JC003008 (2005).
18. D. McKee and A. Cunningham, "Evidence for wavelength dependence of the scattering phase function and its implication for modeling radiance transfer in shelf seas," Appl. Opt. **44,** 126–135 (2005).
19. M. Stramska, D. Stramski, R. Hapter, S. Kaczmarek, and J. Ston, "Bio-optical relationships and ocean color algorithms for

the north polar region of the Atlantic," J. Geophys. Res. **108**(C5), 3143, doi:10.1029/2001JC001195 (2003).
20. A. H. Barnard, W. S. Pegau, and J. R. V. Zaneveld, "Global relationships of the inherent optical properties of the oceans," J. Geophys. Res. **103**(C11), 24955–24968 (1998).
21. R. W. Gould, Jr., R. A. Arnone, and P. M. Martinolich, "Spectral dependence of the scattering coefficient in case 1 and case 2 waters," Appl. Opt. **38,** 2377–2383 (1999).
22. M. Babin, A. Morel, V. Fournier-Sicre, F. Fell, and D. Stramski, "Light scattering properties of marine particles in coastal and open ocean waters as related to the particle mass concentration," Limnol. Oceanogr. **48,** 843–859 (2003).
23. O. Schofield, T. Bergmann, P. Bissett, J. F. Grassle, D. B. Haidvogel, J. Kohut, M. Moline, and S. M. Glenn, "The Long-Term Ecosystem Observatory: an integrated coastal observatory," IEEE J. Oceanic Eng. **27,** 146–154 (2002).
24. G. C. Chang, T. D. Dickey, O. M. Schofield, A. D. Weidemann, E. Boss, W. S. Pegau, M. A. Moline, and S. M. Glenn, "Nearshore physical processes and bio-optical properties in the New York Bight," J. Geophys. Res. **107**(C9), 3133, doi: 10.1029/2001JC001018 (2002).
25. W. J. Rhea, G. M. Lamela, and C. O. Davis, "A profiling optics and water return system for validation and calibration of ocean color imagery," Opt. Express **15,** 2–11 (2007).
26. J. R. V. Zaneveld, J. C. Kitchen, and C. C. Moore, "Scattering error correction of reflecting-tube absorption meters," Proc. SPIE **2258,** 44–55 (1994).
27. D. McKee, A. Cunningham, and S. Craig, "Semi-empirical correction algorithm for AC-9 measurements in a coccolithophore bloom," Appl. Opt. **42,** 4369–4374 (2003).
28. C. D. Mobley, L. K. Sundman, and E. Boss, "Phase function effects on oceanic light fields," Appl. Opt. **41,** 1035–1050 (2002).
29. R. H. Stavn and H. J. Rick, "Correcting the errors from variable sea salt retention and the water of hydration in loss on ignition analysis: coastal and estuarine waters," Estuarine Coastal Shelf Sci. (submitted).
30. S. W. Wright, S. W. Jeffrey, R. F. C. Mantoura, C. A. Llewellyn, T. Bjørnland, D. Repeta, and N. Welschmeyer, "Improved HPLC method for the analysis of chlorophylls and carotenoids from marine phytoplankton," Mar. Ecol. Prog. Ser. **77,** 183–196 (1991).
31. R. R. Bidigare and C. C. Trees, "HPLC phytoplankton pigments: sampling, laboratory methods, and quality assurance procedures," in *Ocean Optics Protocols for Satellite Ocean Color Sensor Validation, Revision 2,* J. Mueller and G. Fargion, eds., NASA Tech. Memo2000-209966 (NASA, 2000), pp. 154–161.
32. A. Morel, "Optical properties of pure water and pure seawater," in *Optical Aspects of Oceanography,* N. G. Jerlov and E. S. Nielson, eds. (Academic, 1974), pp. 1–24.
33. H. Buiteveld, J. H. M. Hakvoort, and M. Donze, "Optical properties of pure seawater," Proc. SPIE **2258,** 174–183 (1994).
34. M. S. Twardowski, E. Boss, J. B. Macdonald, W. S. Pegau, A. H. Barnard, and J. R. V. Zaneveld, "A model for estimating bulk refractive index from the optical backscattering ratio and the implications for understanding particle composition in case I and case II waters," J. Geophys. Res. **106,** 14129–14142 (2001).
35. P. R. Bevington, *Data Reduction and Error Analysis for the Physical Sciences* (McGraw-Hill, 1969).
36. M. Chami, E. B. Shybanov, G. A. Khomenko, M. E.-G. Lee, O. V. Martynov, and G. K. Korotaev, "Spectral variation of the volume scattering function measured over the full range of scattering angles in a coastal environment," Appl. Opt. **45,** 3605–3619 (2006).
37. A. L. Whitmire, E. Boss, T. J. Cowles, and W. S. Pegau, "Spectral variability of the particulate backscattering ratio," Opt. Express **15,** 7019–7031 (2007).
38. H. Loisel, X. Mériaux, J.-F. Berthon, and A. Poteau, "Investigation of the optical backscattering to scattering ratio of marine particles in relation to their biogeochemical composition in the eastern English Channel and southern North Sea," Limnol. Oceanogr. **52,** 739–752 (2007).
39. M. Babin and D. Stramski, "Variations in the mass-specific absorption coefficient of mineral particles suspended in water," Limnol. Oceanogr. **49,** 756–767 (2004).
40. D. Stramski, S. B. Wozniak, and P. J. Flatau, "Optical properties of Asian mineral dust suspended in seawater," Limnol. Oceanogr. **49,** 749–755 (2004).
41. C. H. Whitlock, L. R. Poole, J. W. Usry, W. M. Houghton, W. G. Witte, W. D. Morris, and E. A. Gurganus, "Comparison of reflectance with backscatter and absorption parameters for turbid waters," Appl. Opt. **20,** 517–522 (1981).
42. R. P. Bukata, J. H. Jerome, K. Y. Kondratyev, and D. V. Pozdnyakov, *Optical Properties and Remote Sensing of Inland and Coastal Waters* (CRC Press, 1995).
43. O. Ulloa, S. Sathyendranath, and T. Platt, "Effect of the particle-size distribution on the backscattering ratio in seawater," Appl. Opt. **33,** 7070–7077 (1994).
44. D. Stramski and D. A. Kiefer, "Light scattering by microorganisms in the open ocean," Prog. Oceanogr. **28,** 343–383 (1991).